ELSEVIER

Journal of Membrane Science 99 (1995) 57–75

journal of MEMBRANE SCIENCE

Formation and characterization of supported microporous ceramic membranes prepared by sol-gel modification techniques

R.S.A. de Lange, J.H.A. Hekkink, K. Keizer *, A.J. Burggraaf

University of Twente, Faculty of Chemical Technology, Laboratory for Inorganic Chemistry, Materials Science and Catalysis, P.O. Box 217, 7500 AE Enschede, Netherlands

Received 5 January 1994; accepted in revised form 6 September 1994

Abstract

The formation is described of supported microporous membranes (by IUPAC definition $r_{pore} < 1$ nm), prepared by modification of mesoporous γ-alumina membranes with polymeric sols. The mesoporous γ-alumina membranes, with a top-layer thickness in the order of 7–10 μm, and with pore radii of 2–2.5 nm, have a very high surface finish (mean roughness 40 nm). The amorphous microporous top-layer thickness is in the order of 60–100 nm. Gas transport properties are effectively improved as is shown by activated permeation and molecular sieve-like separation factors in the order of 50–200 for H_2/CH_4. These microporous top-layers can be prepared from a relatively wide range of sol structures; from inorganic oligomers which are too small to result in significant scattering with SAXS, to polymeric structures with fractal dimensions in the range : $1 < d_f < 2.04$, and radii of gyration between 0.8 and 4 nm.

Keywords: Gas separation; Ceramic membranes; Microporous; Sol-gel process

1. Introduction

Since the introduction of inorganic membranes for commercial applications in the early 1970s, the use in many areas such as food and beverage processing, biotechnology and water treatment is expanding rapidly [1]. Nowadays, the interest of applications in emerging areas such as gas separations and membrane reactors is increasing strongly, and due to molecular sieve-like separation properties, especially microporous ($r_{pore} < 1$ nm [2]) membranes are gaining attention [1,3].

The main synthesis routes for microporous ceramic membranes are modification of mesoporous (2 nm $< d_{pore} <$ 50 nm [2]) systems using sol-gel methods [4–10] or by CVD techniques [11–19].

Alternative methods are controlled carbonization of organics for the formation of molecular sieve carbons [20], leaching of hollow glass fibers [21,22], and, more recently, zeolitic membrane systems have been developed [23–26].

In this paper the preparation of microporous membranes by sol-gel modification of mesoporous γ-alumina membranes is described. These γ-alumina membranes are prepared by a dip coating process developed by Leenaars et al. [27,28], which is basically a slip-casting process of a porous support with a colloidal solution of boehmite (γ-AlOOH).

Uhlhorn et al. [29] showed that the introduction of poly(vinyl alcohol) (PVA) in the dip solution improves the membrane quality significantly since defect-free membranes are obtained. Furthermore, the addition of PVA, with molar weight $\leq$ 72 000 Dalton,

* Corresponding author.

SSDI 0376-7388(94)00206-1

did not result in a significant change in microstructure of the top-layer. By control of the dipping time and PVA content, the top-layer thickness can be varied between 1–10 μm.

Modification of these γ-alumina membranes with silica sols was found to result in molecular sieve-like gas transport properties [4,6]. For mesoporous γ-alumina membranes, the main gas transport mechanism for weakly adsorbing gases at temperatures around room temperature or above, is Knudsen diffusion. In Knudsen diffusion the transport rate decreases as function of temperature and the ideal separation factor α^* ($=F_{Kn,0A}/F_{Kn,0B}$) is equal to the inverse square root of the ratio of the molecular masses.

For the modified membranes, however, gas transport was activated with activation energies for hydrogen in the order of 11 kJ.mol^{-1}, and molecular sieve-like separation factors (e.g. α $H_2/C_3H_6 > 272$ at 260°C, and α $H_2/CH_4 = 200$ at 150°C) are reported [4,6]. Due to the very thin top-layer, in the order of 60–90 nm, high permeation rates were obtained. Especially this combination of high permeation rates and high separation factors makes these membranes very attractive for industrial applications. Activated diffusion is typical for microporous materials [3,30,31], and is an elegant way to prove effective modification of mesoporous membranes. The mechanism and microscopic model of micropore diffusion will be analysed and discussed extensively elsewhere [32,33].

It is believed that for obtaining microporous materials using sol-gel technology, weakly branched polymeric sols have to be used [34]. The concept behind this is that interpenetration of the polymeric structures, which takes place during consolidation (drying or thin film formation), leads to very fine pores. From the analysis of fractal structures, which concept was introduced by Mandelbrot [35], it is shown that the mean number of intersections $M_{1,2}$ of two polymeric structures with radius r and fractal dimensions $D_{f,1}$ and $D_{f,2}$ can be expressed as:

$$M_{1,2} \propto r^{(D_{f,1}+D_{f,2}-d)} \qquad (1)$$

where d is the dimension of space ($=3$). The number of intersections can be regarded as the reciprocal of the tendency to interpenetrate. Thus, if the fractal dimension D_f (assume $D_{f,1}=D_{f,2}=D_f$) is lower than 1.5, the number of intersections decreases as r increases, resulting in a higher tendency to interpenetrate for larger structures. This may lead to tiny pores, but also to densification. However, the density of the individual fractal structures is also dependent on fractal dimension and r, as can be seen according to:

$$\text{density} \propto \text{mass/volume} = \frac{r^{D_f}}{r^3} = r^{(D_{f,1}+D_{f,2}-d)} \qquad (2)$$

It is clear that according to relation (2) the density decreases as r is increased. To optimize the microstructure, where a small pore size and a high porosity are preferred, a balance has to be found for these two partly opposing effects.

As shown before [36], we have developed a sol-gel route for the synthesis of weakly branched polymeric SiO_2 sols and binary SiO_2-based sols, with up to 30 mol% TiO_2 or ZrO_2 or 10 mol% $AlO_{1.5}$. The sols have structures ranging from very small oligomeric structures, which are too small to give rise to significant scattering with SAXS, to polymeric sols with fractal dimensions from 1.3 to 2.04 and radii of gyration in the order of 8 to 40 Å. Consolidation of these sols to non-supported membranes showed that these membranes are all microporous or almost dense for nitrogen adsorption [37]. In general, the pore size distributions are bimodal, with a strong maximum at an effective pore diameter around 0.5 nm and a weaker maximum around 0.75 nm.

The relation between sol structure and the final consolidated microstructure, however, could not be explained straightforwardly from an analysis of Eqs. (1) and (2), since for practical situations during membrane formation, the consolidation process is influenced by other processes as well.

If the sol polymers still possess a certain reactivity, then the ratio of the condensation rate to the evaporation rate is important. Slow drying may result in further condensation, leading to more cross-links and therefore to stronger gel structures. The resulting porosity is then high. This is shown in a microstructural comparison between thin films and monoliths prepared from the same weakly branched sol by Frye et al. [38]. It was found that almost dense (2% porosity, from N_2 adsorption) films were obtained, while the microporous bulk sample has a porosity of 16%.

The formation and characterization of these modified membranes is discussed in this paper.

Firstly, some relevant characteristics of the γ-alumina membranes will be presented, where the focus is

on the top-layer which acts as the support for the microporous layer. The microstructure of the γ-alumina layer is expected to be a very important parameter which determines the final quality of the supported microporous top-layer. Secondly, the characterization of the microporous top-layer is discussed, where the focus is on layer thickness and structure. The range in which supported membranes can be formed is discussed based on results from gas transport experiments.

2. Experimental

Boehmite (γ-AlOOH) sols were used for the formation of mesoporous γ-alumina membranes [29]. Supported γ-alumina membranes were prepared by a dip coating process of α-alumina supports (disc-shape, diameter 39 mm, thickness 2 mm, mean pore radius 160 nm, porosity 50%, polished with 800 grid sandpaper) in boehmite dip solutions as described extensively elsewhere [28,29].

Non-supported γ-alumina membranes were prepared by pouring the dip solutions in petri-dishes, followed by overnight drying in the climate chamber (Hereaus Vötch VTRK 300) and calcining procedures analogous to the procedures for supported membranes. These non-supported membranes are prepared for the characterization of the pore structure with adsorption–desorption techniques. The amount of top-layer material in the supported membrane is too small to characterize the pore size distribution quantitatively with the adsorption–desorption technique.

Polymeric SiO_2 sols were prepared by acid catalysed hydrolysis of tetraethylorthosilicate (TEOS, Merck, p.a. grade) in ethanol with standard molar ratios of 1:6.4:0.085:3.8 TEOS–water–HNO_3–ethanol (sample code: $StSiO_2$). The sols were prepared by careful dropwise addition of water and acid to the TEOS–ethanol solution, followed by 3 h refluxing at 80°C under stirring.

Binary sols were prepared using titanium isopropoxide [$Ti(O^iPr)_4$, Merck, p.a. grade] or titanium *n*-butoxide [$Ti(O^nBu)_4$, Merck, p.a. grade], zirconium–*n*-butoxide–*n*-butanol complex [$Zr(O^nBu)_4$–^{n}BuOH, Alfa, p.a. grade] and aluminium–di-*sec*-butoxide–acetoacetic ester chelate [$Al(O^sBu)_2$–etac, Alfa, p.a. grade] as alkoxides for SiO_2/TiO_2, SiO_2/ZrO_2 and SiO_2/Al_2O_3, respectively. A prehydrolysis process, as described in detail elsewhere [36], has been developed for the synthesis of binary sols. This process involves a prehydrolysis step of the relatively slowly reacting TEOS prior to the addition of the highly reactive transition-metal alkoxides. As a consequence, homogeneous polymeric binary sols will be obtained. Sample codes are given as SiM10, where M is the binary component (Ti, Zr, Al) and 10 represents the molar percentage MO_x (10%).

γ-Alumina membranes were modified by a dip coating process, analogous to γ-alumina membrane preparation, using freshly prepared, ethanol diluted SiO_2 sols and binary sols with a final oxide concentration of 0.1 mol MO_x per liter. The standard dipping time is 4 s. The membranes were allowed to dry for about 30 s, followed by calcination under static air for 3 h at 400°C (heating and cooling rates, 25°C.h).

Membrane codes for silica modified membranes are given as Al*x*-Si*y*-*z*, where *x* represents the number of γ-alumina layers, *y* the number of silica layers, and *z* refers to the membrane under discussion. Composite modified membrane codes are given as Al3-*sol*, where *sol* represents the used binary sol.

2.1. Characterization techniques

N_2 adsorption–desorption (77 K) experiments on non-supported γ-alumina membranes were performed using a MicroMeritics ASAP 2400 adsorption–desorption equipment. Pore size calculations were performed according to the model of Barret, Joyner and Halenda (BJH) [39], which assumes cylindrical pore geometry and includes length and area of the pore walls. For the assessment of the slit-width, in case of slit-shaped pore geometry, the pore size at the inflection point in the desorption branch of the hysteresis loop is taken to calculate the Kelvin radius (r_K), where the Kelvin equation, for nitrogen adsorption at 77 K, is given according to: $r_K = 0.408/\log(P_0/P)$ [40]. The cylindrical pore radius ($r_{p,cyl.}$) can be calculated by [2]:

$$r_{p,cyl.} = r_K + t \tag{3}$$

For slit-shaped pore geometry, the slit width ($d_{p,slit}$) is given by [2]:

$$d_{p,slit} = r_K + 2.t \tag{4}$$

where t is the thickness of the adsorbed layer at the inner surface of the pore, the so-called "t-layer" [40].

For the calculations, the desorption branch of the isotherm is used since it determines the size of smallest pore constrictions.

Permporometry experiments on supported γ-alumina membranes were performed on a home-made equipment as described elsewhere [41]. The oxygen permeation through the membrane is measured as function of the relative vapor pressure of cyclohexane. The experiment is performed in the desorption mode. At high pressures all the pores are blocked by condensed cyclohexane. By decreasing the relative vapor pressure, first the larger pores will be opened and oxygen can permeate. Since the relative vapor pressure corresponds to a certain Kelvin radius, a pore size distribution can be calculated from a plot of oxygen permeation as function of Kelvin radius. Characterization of microporous membranes with this technique, however, is not possible since at very low relative pressures micropore filling takes place and the concept of t-layer and meniscus cannot be used [2,39].

Characterization of the surface roughness of γ-alumina and silica modified-γ-alumina membranes were performed with profilometry (Dektak 3030, Sloan Technology Corporation) and atomic force microscopy (AFM, Nanoscope II). The radius of the tip used for AFM was about 10 nm. Layer thickness characterization was performed using conventional scanning electron microscopy (SEM, Jeol JSM 35-CF) and field-emission SEM (Hitachi S800).

For the ultra-thin microporous films, sputter profiles obtained with X-ray photo spectroscopy (XPS, Kratos XSAM 800) and scanning Auger microscopy (SAM, Perkin–Elmer PHI 600) were used as well for layer thickness characterization. Sputter rates (by Ar^+-ion bombardment) for both experimental techniques are calculated from the calibrated sputter rate for dense Ta_2O_5. The relative sputter rate of dense SiO_2 compared to Ta_2O_5 is 0.85 [42]. The order of the sputter rates for SiO_2 is around 3 $nm.h^{-1}$ for XPS and 150 $nm.h^{-1}$ for SAM. The sputtered areas are 8×8 mm for XPS and 1.5×1.5 mm for SAM, while the spot sizes for analysis are 3 mm and 0.5–1 μm diameter, respectively. The information depth for these techniques is in the order of 5 nm [43]. Due to the insulating nature of SiO_2, charging of the sample surface can occur during auger analysis. This could be avoided by tilting the samples at an angle of 50° and the use of a very low current of 10 nA (accelerating voltage of 3 kV). Also the samples were covered with gold (thickness 200 Å), where a spot of around 2×2 mm was left free for the analysis.

Gas permeation experiments were performed by measurement of dead-end permeation with equipment as described elsewhere [32]. The disc-shaped membranes were placed in stainless steel cells (Velterop b.v., R 250), with the top-layer at the feed side. Kalrez (DuPont) sealings were used, with a measuring area of 1.911 cm^2, and maximum process temperature 300°C. The gas flow ($ml.min^{-1}$) through the membrane was controlled by a mass-flow controller (Brooks, 5051); feed pressure and pressure difference over the membrane were measured using pressure transducers (Validyne). The low pressure side of the membrane was evacuated ($P < 0.01$ bar).

The permeation (F) [1] is expressed in $mol.m^{-2}.s^{-1}.Pa^{-1}$ in cases where a linear relation between membrane flux and pressure was proven. Correction of the modified membrane permeation rates for the support influence are performed according to the method as described in the Appendix.

Gas separation experiments were performed using binary gas mixtures in equipment as described extensively elsewhere [32]. Experiments were performed in counter-current mode, in stainless steel membrane test cells (Velterop b.v., R 250), with Kalrez sealing and a measuring area of 1.911 cm^{-2}. The binary gas mixture was led along the microporous top-layer at the high pressure side and argon was used as sweep gas at the permeate side, which was connected to a vacuum pump.

The separation factor (α), defined as the enrichment factor of one component in the permeate compared to feed composition, is given by Eq. (5):

$$\alpha = \frac{y}{1-y}\frac{1-x}{x} \tag{5}$$

where y is the molar fraction of the faster permeating component in the permeate and x is the molar fraction of this component in the feed.

Microporous membranes were degassed prior to the permeation and separation measurements, in order to remove adsorbed water from the micropores, by overnight heating to 200°C with a hydrogen flow of 1 $ml.min^{-1}$ and the low pressure side connected to the vacuum pump. The gases used were >99.9% pure.

[1] 1 $mol.m^{-2}.s^{-1}.Pa^{-1} \equiv 1.344\ 10^7$ $ml.min^{-1}.cm^{-2}.bar^{-1} \equiv 1.93\ 10^8$ $m^3.m^{-2}.day^{-1}.bar^{-1}$.

3. Results

3.1. Pore size characterization of non-supported γ-alumina membranes

Results of N_2 adsorption–desorption experiments on several non-supported γ-alumina have been summarized in Table 1. Samples AI and BI were prepared from standard 0.6 M AlOOH dip solutions, which were dried overnight in the climate chamber, and calcined according to the standard procedure (3 h, 600°C; 60°C.h^{-1} heating and cooling rate). Sample CI was prepared from a 0.3 M AlOOH dip solution, with the other conditions, such as PVA content, kept constant. Samples AII, BII and CII were prepared as samples AI, BI and CI, but dried in the laminar flow cupboard. Due to the lower drying rate, it took 2–3 days to dry these samples. Samples D, E and F were obtained by a second calcination procedure of different fractions of sample BI for, respectively, 3 h, 700°C; 6 h, 700°C and 3 h, 750°C; heating and cooling rates were 60°C.h^{-1}.

The isotherms and pore size distributions of samples AI and CII, which are representative for this set, are given in Figs. 1 and 2, respectively. The isotherm shape is typically of type IV [2,39], which is ascribed to mesoporous solids. The hysteresis loop is of type H2 [2]. However, it is difficult to ascribe this hysteresis type to a certain pore size and shape, since it has been observed for many porous solids of different nature. It is believed in literature that network effects must be taken into account [2]. However, based on TEM observations and liquid permeation, it was expected by Leenaars and Uhlhorn that the pore shape is likely to be slit-shaped [27–29].

Pore size calculations are performed according to cylindrical geometry (BJH method [39]), where the average pore size is given (Av. $r_{p,des}$), and from the calculation of the Kelvin radius from the inflection point of the desorption branch, using cylindrical geometry ($r_{cyl.}$) and slit shape geometry (d_{slit}) to calculate the corresponding pore size.

From Table 1 it can be seen that the slower drying rate for the samples placed in the laminar flow cupboard compared to the samples dried in the climate chamber results in only slightly lower pore sizes, but comparable pore volumes and surface areas. The effect of AlOOH concentration, however, is much stronger. 0.3 M AlOOH dip solutions result in around 10–15% larger pore sizes and pore volumes. The total volume adsorbed (Fig. 1) for sample CII is considerably higher than for sample AI, and the hysteresis loop is shifted to higher relative pressures, which implies larger pore sizes, as can be seen in Fig. 2. The shape of both the isotherm and the hysteresis loop is not changed.

The influence of the second calcination procedure is only very minor for the conditions studied. As can be seen in Table 1, the average pore radius (BJH)

Table 1
Results of N_2 adsorption–desorption measurements on non-supported γ-alumina membranes

Sample	S_{BET} (m^2.g^{-1})	$V_{p,des}$ (ml.g^{-1})	Porosity[a] (%)	Average $r_{p,des}$ BJH[b] (nm)	P/P_0^c inflection	$r^d_{cyl.}$ (nm)	d^e_{slit} (nm)
AI, 3 h, 600°C	262	0.352	56	1.88	0.549	2.18	2.80
AII, 3 h, 600°C	282	0.362	57	1.84	0.539	2.13	2.74
BI, 3 h, 600°C	288	0.375	58	1.84	0.539	2.13	2.74
BII, 3 h, 600°C	267	0.341	56	1.8	0.521	2.05	2.65
CI, 3 h, 600°C	286	0.438	62	2.19	0.585	2.39	3.03
CII, 3 h, 600°C	287	0.43	61	2.09	0.581	2.37	3.01
D, 3 h, 700°C[f]	267	0.358	57	1.86	0.545	2.16	2.77
E, 6 h, 700°C[f]	244	0.347	56	1.96	0.561	2.25	2.87
F, 3 h, 750°C[f]	198	0.341	56	2.37	0.626	2.67	3.34

[a] $\rho_{\gamma\text{-alumina}} = 3.7$ g.cm^{-3}.
[b] Average pore radius after Barret, Joyner and Halenda [41].
[c] $r_K = 0.408/\log(P_0/P)$, t after [42].
[d] Cylindrical geometry: $r_{cyl.} = r_K + t$.
[e] Slit-shaped geometry: $d_{slit} = r_K + 2t$.
[f] Second calcination procedure, first step: 3 h, 600°C (sample BI).

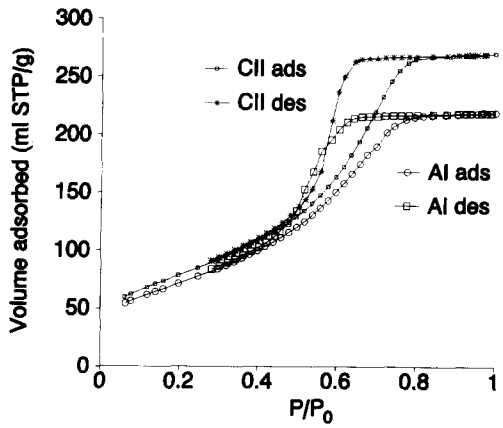

Fig. 1. N_2 adsorption–desorption isotherms of γ-alumina samples CII and AI.

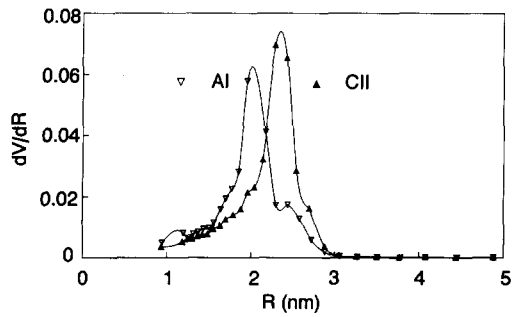

Fig. 2. Pore size distributions of γ-alumina samples CII and AI.

increases only from 1.84 nm (BI, 600°C) to 2.37 nm (F, second step: 3 h, 750°C). The pore volume is then decreased by about 9%. Also it can be seen that the pore growth and pore volume decrease for sample F (second step: 3 h, 750°C) is much larger compared to sample E (second step: 6 h, 700°C) due to the higher calcination temperature.

3.2. *Pore size characterization of supported γ-alumina membranes*

The oxygen permeation and the calculated pore size distribution (PSD), obtained by permporometry, for a representative supported γ-alumina membrane, sample AI3, is shown in Fig. 3. The membrane was prepared according to the standard synthesis route, where the γ-alumina layer was deposited in three dipping steps. Calcination took place at 600°C for 3 h. In Fig. 4, the permporometry results of the same membrane are shown after a second calcination step (3 h, 700°C).

The calculated PSDs give the distribution of the total *number* of pores within a certain range. It can be seen that the permeation at large Kelvin radii is almost zero, and that a strongly increased permeation is observed around 2–2.5 nm. This implies that no or only a few pores are present with Kelvin radii larger than 2.5 nm. The weak increase in permeation at Kelvin radii smaller than 2 nm can be ascribed to the decrease of the t-layer thickness [40]. It can be seen that the PSD is slightly sharper and shifted to larger pore sizes after the second calcination step.

The calculated maxima are given in Table 2, and are found at $r_K = 2.0$ nm and at $r_K = 2.3$ nm. The effective pore sizes for cylindrical pore geometry and slit shape pore geometry can be calculated with Eqs. (3) and (4), respectively, where the mean thickness of the monolayer can be estimated to be approximately 0.5 nm [40,44]. As can be seen by comparison with the

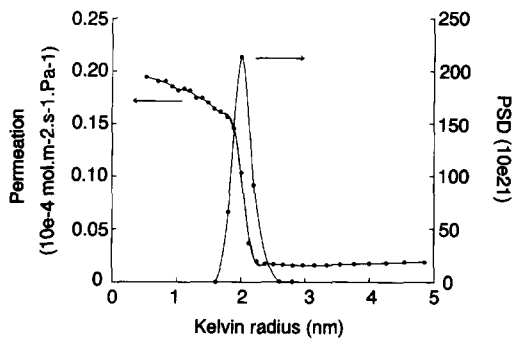

Fig. 3. Oxygen permeation and PSD (by number) as function of Kelvin radius for γ-alumina membrane AI3, calcined at 600°C, determined with permporometry.

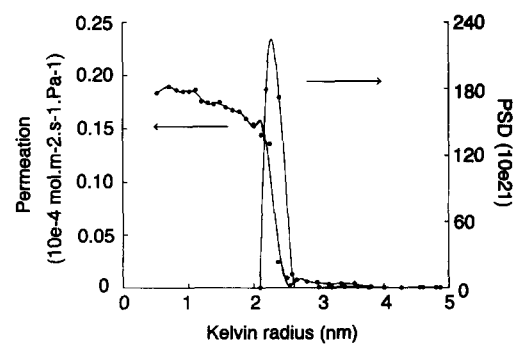

Fig. 4. Oxygen permeation and PSD (by number) as function of Kelvin radius for γ-alumina membrane AI3, after the second calcination step at 700°C, determined with permporometry.

Table 2
Calculated maxima in PSD (by number) of supported γ-alumina membrane Al3 obtained with permporometry[a]

Calcination procedure γ-alumina	r_K (nm)	$r^b_{cyl.}$ (nm)	d^c_{slit} (nm)
3 h, 600°C	2.0	2.5	3.0
3 h, 600°C + 3 h, 700°C	2.3	2.8	3.3

[a]t-layer thickness ≈0.5 nm [46].
[b]$r_{cyl.} = r_K + t$.
[c]$d_{slit} = r_K + 2t$.

results obtained for non-supported membranes in Table 1, the pore sizes for the supported membrane, as calculated by permporometry, are slightly higher after calcination at 600°C (compare with samples AI and BI), and after the second calcination at 700°C (compare with sample D). It should be noted, that permporometry only measures the pores which contribute to the flow, dead-end pores do not contribute to the distribution, contrary to N_2 adsorption–desorption.

3.3. Surface morphology characterization of γ-alumina membranes

A typical cross-section of a γ-alumina membrane is shown in Fig. 5. The membrane was prepared by three dipping procedures. The top-layer thickness for this membrane is around 8–9 μm. The mean thickness for membranes after 3 dipping procedures was found to be 7–10 μm, where the thickness of the individual layers is between 2 and 3 μm. In ideal cases, related with sample preparation for SEM, these individual layers can be seen as showed by Zaspalis [45].

It can be seen clearly that the γ-alumina layer decreases the support roughness, which decrease is already obtained for the largest part after the first dipping step. Roughness measurements with profilometry showed that the mean roughness (defined as the mean deviation from the baseline for a certain scan length) for scan lengths of around 1 mm is in the order of 40 nm. Surface roughness measurements with AFM showed the same mean roughness of 40 nm for scan lengths of around 1 μm.

3.4. Surface morphology characterization of silica modified membranes

A three-dimensional AFM picture of a silica modified γ-alumina membrane is shown in Fig. 6. The experiment was performed in the so-called constant force mode, where the (electrostatic, Lennard-Jones type) repulsion force between sample and tip is maintained at zero. As can be seen clearly, the top-layer shows a surface roughness with maxima of around 20–40 nm, which is only slightly better than the surface roughness of γ-alumina membranes.

Layer thickness characterization of silica modified γ-alumina membranes is performed with SAM, and for a single experiment with XPS, by the analysis of argon sputter profiles. The dipping time was varied from 2 to 8 s. All samples were calcined for 3 h at 400°C (heating and cooling rates of 25°C.h^{-1}). Also multiple SiO_2 dipping experiments have been included. These membranes were first modified according to the standard procedure, with 4 s dipping time. After calcination a second modification was performed under identical conditions. The main goal of a second modification step is to repair possible pin-holes and/or cracks, analogous to the repair of γ-alumina membranes [29]. The digit in the used sample codes for these experiments refers to the dipping time in seconds (4-4 refers to the multiple dipped membranes), followed by a character to distinguish for the individual samples.

Representative SAM and XPS sputter profiles, for silica modified γ-alumina membrane 4C, are shown in Figs. 7 and 8, respectively. Membrane 4C is prepared by dipping a standard γ-alumina membrane for 4 s. In the SAM sputter profiles in Fig. 7 the relative concentrations of Al and Si are given as function of the sputter depth. The concentrations are calculated both from the LMM electrons and the KLL electrons. The resulting profiles resemble each other strongly. As can be seen, the concentration Si starts decreasing at a sputter depth of around 25 nm, and at 45 nm a cross-over point in relative concentration is present. At 60 nm no silicon can be detected. The XPS sputter profile in Fig. 8, which also includes the oxygen concentration, has the same shape. The total thickness is equal, however, the cross-over point is at 35 nm, which is slightly less compared to the SAM profile. The stoichiometry for both silica and alumina was found for this experiment to be around $MO_{2.5}$. However, the determination of the correct stoichiometry is not reproducible due to errors in the detected oxygen concentration. Therefore, only the relative concentrations of aluminium and silicon are discussed.

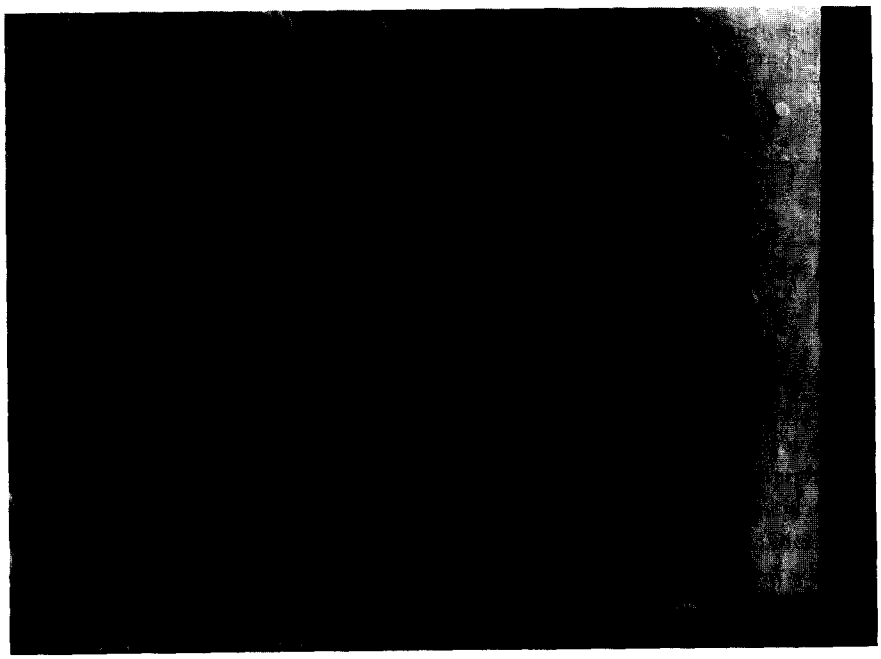

Fig. 5. SEM-micrograph of a cross-section of a three times dipped γ-alumina membrane.

Results for samples with different dipping times have been summarized in Table 3. For some samples, duplicate experiments, by taking two parts of the same membrane, have been performed. From Table 3 it can be seen that for a single membrane, the layer thickness seems to be uniform and the measurement is reproducible. Between different membranes, however, a variation in layer thickness of a factor two can occur.

The influence of the change of dipping time on layer thickness is, within the experimental error, negligible in the dipping time range of 2–8 s.

Multiple dipping of silica membranes with standard sols showed visible cracking of the top-layer in some cases, which was observed by conventional light microscopy. The membranes given in Table 3 did not show any cracking. Remarkable is that the layer thick-

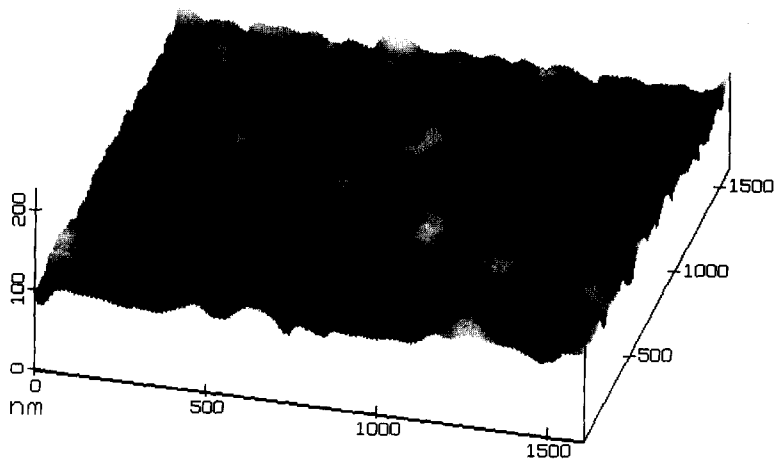

Fig. 6. Three-dimensional AFM picture of silica-modified membrane.

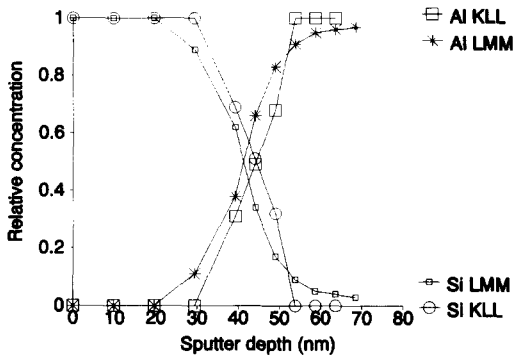

Fig. 7. SAM sputter profile silica modified γ-alumina membrane 4C.

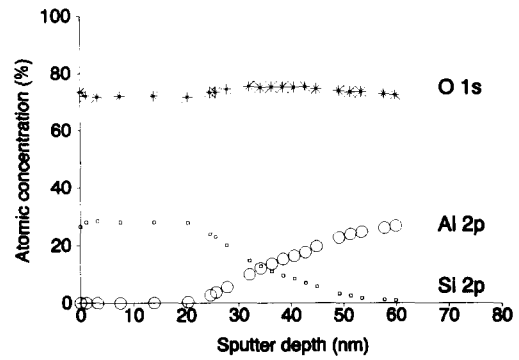

Fig. 8. XPS sputter profile silica modified γ-alumina membrane 4C.

ness is only very slightly increased compared to the single dipped membranes.

In Fig. 9, a FE-SEM picture is shown of silica modified γ-alumina top-layer (membrane 4F). A very nice layer can be seen with a thickness of around 120 nm, which is in agreement with the results found for SAM and XPS.

3.5. Gas transport characterization of microporous membranes

Pure SiO_2 modified membranes

The H_2 permeation and CO_2 permeation as function of temperature for silica modified membrane Al3-Si1-D are shown in Figs. 10 and 11, respectively. The membrane fluxes for both gases were linearly dependent on pressure, which result in practically pressure independent permeation rates. As can be seen, the permeation increases as function of temperature both for H_2 and CO_2. This is a clear evidence that an effective modification with a microporous top-layer is obtained, since gas permeation rates according to Knudsen diffusion or surface diffusion will decrease for increased temperatures. The calculated activation energies for permeation for the membrane system (≡ γ-alumina membrane + microporous SiO_2 top-layer) are 11.0 kJ.mol^{-1} for H_2 and 2.0 kJ.mol^{-1} for CO_2. Correction for support (≡ γ-alumina membrane) influence gives the true apparent activation energies for the silica top-layer, which are slightly higher; 12.3 kJ.mol^{-1} and 2.7 kJ.mol^{-1} for H_2 and CO_2, respectively.

Table 3
Layer thickness of microporous SiO_2 top-layer obtained by SAM sputter profiles

Membrane 4 s dipping	Cross-over depth (nm)	Total layer thickness (nm)	Membrane 2, 8, 2x4 s dipping	Cross-over depth (nm)	Total layer thickness (nm)
4A	40	60	2A	65 90	80 100
4B	50	75	2B	48 62	70 80
4C	45	60	8A	95 75	120 90
4C[a]	35	60	8B	78 70	100 100
4D[b]	≈25	60	4-4A[c]	90	110
4D[a,b]	90	>90	4-4B[c]	110	140
4E	82 82	100 100			
4F[d]		120			
4G[d]		150			

[a]Obtained from XPS-sputter profiles.
[b]Data taken from Uhlhorn [4].
[c]Prepared in 2 modification steps with intermediate calcination.
[d]Obtained from FE-SEM.

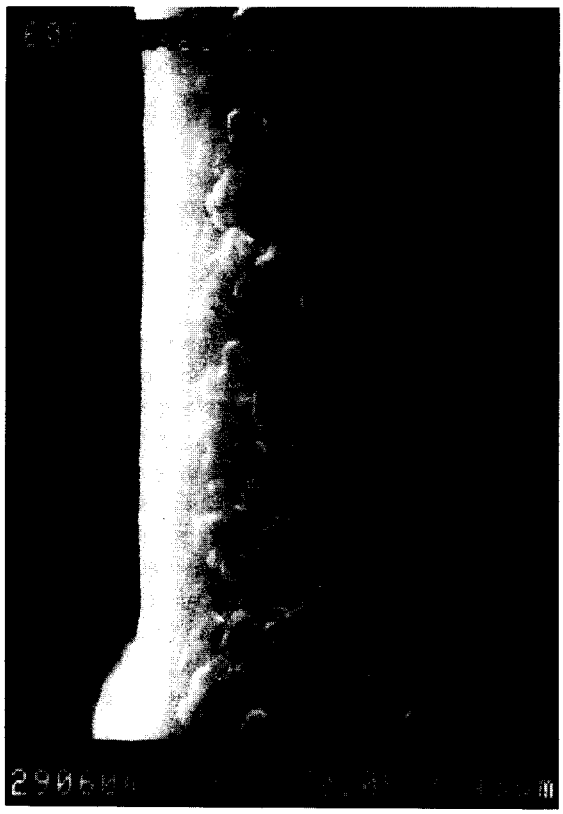

Fig. 9. FE-SEM micrograph of a cross-section of a γ-alumina top-layer modified with silica.

The effect of support correction is clearly shown for membrane Al3-Si2-A. This membrane was prepared by multiple modification with silica of a γ-alumina (3 layer) membrane. The second dipping procedure was intended to repair possible cracks and/or pinholes. The dip solution for this second step was prepared by diluting a standard sol 180 times, which is 10 times more diluted than for standard modification procedures for the first step. By using these very diluted sols no cracking of the top-layer was observed.

After the first modification the permeation rate for H_2 at 50°C was around 3.7×10^{-7} mol.m^{-2}.s^{-1}.Pa^{-1} (single point measurement). The H_2 permeation *after the second modification* step is shown in Fig. 12, where both the membrane (γ-alumina membrane + silica top-layer) permeation (M) and the top-layer (microporous silica) permeation (T), obtained by support correction, are given. The permeation rate for H_2 at 50°C is decreased by almost a factor two due to the second modification step. The difference between the membrane system permeation and corrected top-layer permeation increases with temperature. This is caused by the increased top-layer permeation at higher temperatures (due to activated transport), and the decreased support permeation, which follows Knudsen diffusion [Eq. (1)]. Therefore, the difference in permeation rates for support and top-layer decreases, resulting in a stronger contribution of the support to the total pressure drop over the membrane. Consequently, corrections become more important at higher temper-

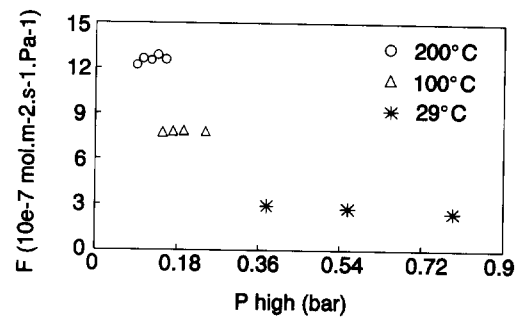

Fig. 10. H_2 permeation for silica modified membrane Al3-Si1-D.

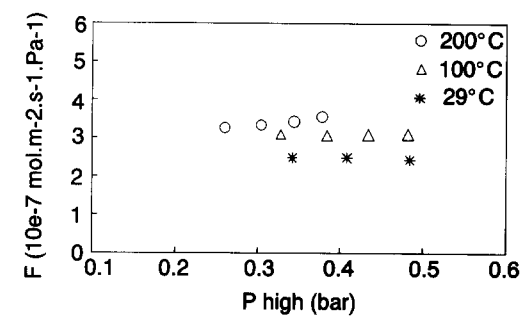

Fig. 11. CO_2 permeation of silica modified membrane Al3-Si1-D.

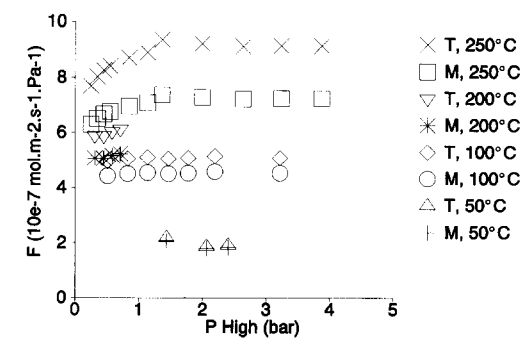

Fig. 12. H_2 permeation of silica modified membrane Al3-Si2-A (M) and microporous top-layer (T), after the second dipping step.

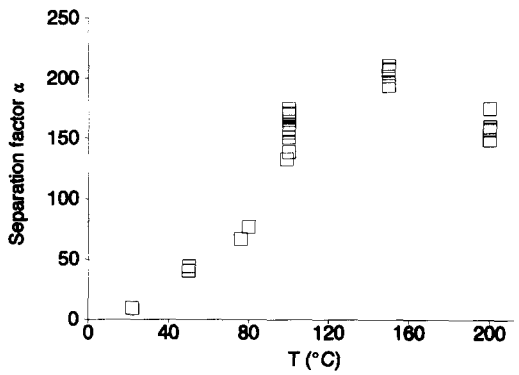

Fig. 13. H_2/CH_4 and H_2/CO_2 separation results for silica modified membrane Al3-Si2-A prepared by a multiple dipping procedure.

atures. This can be clearly seen in the example in the Appendix. As a consequence, the calculated activation energy for permeation for the top-layer (8.2 kJ.mol^{-1}) is higher than for the total membrane system (7.1 kJ.mol^{-1}).

Also it can be seen that the permeation is practically pressure independent up to 4 bar feed pressure, apart from the data points at high temperature at low pressures. The latter effect is attributed to the lower accuracy of the pressure transducers at these low pressures.

In Fig. 13 results are shown for separation experiments of H_2/CO_2, obtained after the first modification, and of H_2/CH_4, both after the first modification and the second modification step. The feed pressure was 2.7 bar and the pressure difference was 1.9 bar for these experiments. The feed composition was 50:50 with a

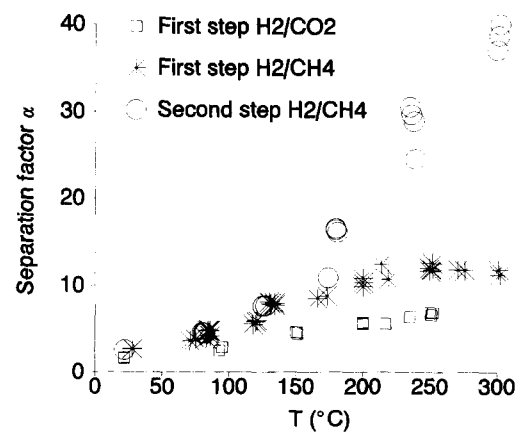

Fig. 14. H_2/CH_4 separation of microporous silica/titania modified membrane Al3-SiTi10X.

flow rate of 100 ml.min^{-1}. The argon sweep gas flow rate was 150 ml.min^{-1}.

After the first modification step with silica, both the H_2/CO_2 separation factor and the H_2/CH_4 separation factor increase as function of temperature. The absolute value is for both sets higher than the ideal separation factors according to Knudsen diffusion, which are 4.69 for H_2/CO_2 and 2.83 for H_2/CH_4. The absolute separation factors, as well as the improvement of the separation factors compared to Knudsen diffusion, are higher for the H_2/CH_4 combination.

A considerable improvement of the separation factor is obtained after the second modification step. The H_2/CH_4 separation factor at 300°C is increased from around 12 to 40.

Composite SiI_2/TiO_2 and SiO_2/Al_2O_3 modified membranes

Membrane Al3-SiTi10X was modified with binary SiO_2/TiO_2 (10 mol% TiO_2) sol SiTi10X. This sol was prepared by mixing of a SiO_2 sol and a TiO_2 sol, which were separately prehydrolysed, as described extensively elsewhere [36]. SAXS analysis showed that the fractal dimension of this sol was 2.04 (after 30 days) with a radius of gyration of 36 Å. The dried and calcined non-supported film was almost dense (porosity 2%) [37]. Microporous membranes "Al3-SiTi10Bu2", "Al3-SiTi10Pr2" and "Al3-SiAl10 $r_w = 4.6$, 70" were prepared by the modification of γ-alumina membranes with the corresponding binary sols. The SiO_2/TiO_2 sols "SiTi10Bu2" and "Siti10Pr2" were prepared by a so-called *two step hydrolysis* process, which involves a second hydrolysis step after the addition of the titanium alkoxide to the prehydrolysed SiO_2 sol [36]. The fractal dimensions are 1.3 and the radii of gyration are 17 Å for both "SiTi10Bu2" and "SiTi10Pr2". Sol "SiAl10 $r_w = 4.6$, 70" was prepared by a single step prehydrolysis process. SiO_2/Al_2O_3 sols prepared under comparable conditions showed no significant scattering in the SAXS experiments, which implies that very small oligomeric structures have been obtained.

The porosity of the microporous non-supported membranes was 28% and 27% for SiTi10Bu2 and SiTi10Pr2 respectively; non-supported membrane SiAl10 $r_w = 4.6$ was practically dense for nitrogen (porosity 1%) [37].

Table 4
Selected gas transport properties of microporous sol-gel derived membranes

Membrane	F_{H_2} [a], 200°C	F_{CO_2} [a], 200°C	E_{act}, H_2 [b] (kJ.mol^{-1})	E_{act}, CO_2 [b] (kJ.mol^{-1})	α[c] H_2/CH_4
Al3-Si1-D	13	3.5	11.0 (12.3)	2.0 (2.7)	
Al3-Si1-A-(2)[d]	5.2		7.1 (7.9)		5 (100°C)
					18 (200°C)
					40 (300°C)
Al3-SiTi10Bu2	7.4	0.8	7.0 (8.4)	1.4 (1.7)	
Al3-SiTi10Pr2	13.1	1.6	12.3 (16.3)	2.6 (3.9)	
Al3-SiAl10	2.3	0.5	9.0 (9.2)	6.0 (6.5)	
r_w = 4.6, 70					
Al3-SiTi10X	≈ 1				40 (50°C)
					160 (100°C)
					200 (150°C)
					160 (200°C)

[a]Permeation in 10^{-7} mol.m^{-2}.s^{-1}.Pa^{-1}. Linear relation between F and feed pressure up to at least 3–4 bar.
[b]Values between parentheses corrected for support influence.
[c]Obtained from separation experiments with binary gas mixtures.
[d]Data obtained after the second modification step.

H_2/CH_4 separation results for Al3-SiTi10X are shown in Fig. 14. A 50:50 feed, with a total flow rate of 200 ml.min^{-1} was used. The argon sweep gas flow rate was 200 ml.min^{-1}. The feed pressure was 3.1 bar and the pressure difference over the membrane was 1.8 bar. This membrane shows extremely high H_2/CH_4 separation factors. Obviously the binary sol resulted in a microporous top-layer. As can be seen, an optimum in separation factor, is present at 150°C.

In Table 4 some gas transport data have been summarized. The binary membranes showed activated transport as well, with activation energies in the order as have been found for silica modified membranes.

4. Discussion

As shown in Table 1, the lower AlOOH concentration in the dip-solutions (standard: 0.6 M AlOOH), results in higher pore volumes and a slightly increased pore size. The PVA content for these sols, however, was not changed. Therefore, another important difference between the 0.6 M sol and 0.3 M sol is the ratio PVA:sol. Since the amount of PVA was kept constant, this ratio is twice as high in the 0.3 M dip solution. An explanation may be that the application of a high PVA:sol ratio leads to a certain amount of destabilization of the sol particles [46]. This results in a less dense packed consolidated gel, and therefore higher pore volume and pore size. More work is currently going on to investigate the influence of PVA more extensively.

Comparison of the data obtained for non-supported membranes with supported membranes can be performed elegantly by the use of permporometry. As can be seen in Table 2, the calculated pore sizes are slightly higher for the supported membranes. As has been noted before, one has to recognize that permporometry characterizes only the "active" pores for permeation, dead-end pores are therefore not detected. This can lead to higher mean pore sizes for permporometry.

A second explanation for the slightly higher pore size for the supported system can be given based on the effect of support constraints for the supported membranes. For supported TiO_2 membranes, it was shown by Kumar et al. [47] that support constraints hinder the densification and phase transformation significantly. While for non-supported membranes the porosity was around 15–20%, the supported membranes showed a porosity of about 25–30%. The phase transformation for anatase to rutile was shifted from 650°C to about 850°C. Shrinkage of the top-layer, due to either drying or sintering, results in additional tensile stresses in the top-layer originating from the rigid support. These additional stresses reduce the drying stresses and sinter stresses, which are both compressive. The sup-

port effect was also partly attributed to the possibility of particle rearrangement, which is less for the supported membranes.

The surface roughness values for γ-alumina are comparable with results from earlier work [48,49], where it was shown that both the ground support (800 grid sandpaper) and the γ-alumina membranes have the same roughness of 40 nm. This final roughness looks to be an intrinsic property of the γ-alumina layer, since it cannot be improved even after multiple dipping procedures. The roughness was also not decreased, within the experimental error by the silica top-layer as we have shown.

The mean roughness of the silica top-layer and the γ-alumina membrane may be the explanation for the gradual decrease of the silica concentration as found in the sputter profiles measured with SAM and XPS. Since a relatively large area, compared to the surface roughness, is scanned during analysis, the γ-alumina layer will appear gradually during sputtering. Because of the surface roughness of around 40 nm, a cross-over region can be expected of the same order, provided the order of the sputter rates for SiO_2 and Al_2O_3 are comparable, which is the case for Al and Si [50].

Another possibility can be partly penetration of the silica in the γ-alumina pores. Since the difference between the pore diameter (around 3 or 5 nm for slit-shaped geometry or cylindrical geometry respectively) and radius of gyration of the weakly branched silica sols (R_g around 2 to 3 nm) is not very large it is not expected that penetration takes place very deep into the γ-alumina pores. Condensation and gelation will take place in the pores, and consequently the further transport of the sol particles within the layer is hindered.

As can be seen from Table 3, the variation in layer thickness of silica membranes dipped for 4 s is between 60 and 100 nm. There is no significant difference, within the experimental error, in the layer thickness for membranes dipped for 2 s and for 8 s. Several effects may be responsible for this. When film formation takes place mainly by film coating, and slip casting is a very minor contribution, then the dipping time is not relevant but factors such as sol viscosity, pulling speed and surface tension are dominant [34]. Most probably slip casting is of minor importance because the resistance of flow of liquid through the formed microporous gel layer is very high and consequently the slip cast rate is low.

Since dipping takes place manually, pulling speed variations are a possible source of the scatter in layer thicknesses in the film coating process. The preliminary results presented for membranes which were modified in two steps can, within the experimental error, also be explained by this formation mechanism.

On the other hand, if slip-casting is important, the layer thicknesses would then theoretically have the ratio 1:1.41:2 for membranes dipped for 2, 4 and 8 s, since the layer thickness is proportional to the square root of the dipping time [28,29]. From the data available, we have to conclude that it is not likely that slip-casting is the *dominant* layer formation process.

Comparison of data obtained with SAM and XPS with FE-SEM cross-sections shows that the order of the calculated membrane thickness is comparable. An important cause for possible errors in the absolute calculated layer thickness from sputter profiles can be the estimate for the sputter rate. This is based on dense SiO_2, whereas the membranes are porous. The comparison of the three techniques shows that no large error in the assessment has been made.

Since the membrane layer thickness is in the same order of the mean surface roughness of the support (40 nm), we believe that the quality of the support is a very important condition for successful membrane modification. Commercially available mesoporous ceramic membranes, which are mainly tubular systems, are generally of much lower surface quality, and will consequently need additional intermediate layers of better quality before modification can be successfully performed.

The application of a second modification step is an effective method to repair the membrane quality, which has also been found for γ-alumina membranes by Uhlhorn et al. [29]. The picture which was proposed to explain this, was that during the second slip-casting step of the γ-alumina layer with boehmite (same concentration in first and second step), initially preferential deposition of a gel layer takes place at a defect, since the permeation at these places is higher than on defect-free γ-alumina.

As we have shown, the concept of membrane repair by a second dipping procedure can be applied as well for sol-gel derived microporous membranes (Fig. 13). The hydrogen permeation rate has decreased by a factor two and the separation factor was improved significantly. Since the sol concentration is very low for the

Table 5
Comparison of sol properties, non-supported membrane characteristics and supported membrane characteristics.

	Sol SAXS			Nonsupported[a]		Supported[a]	
	age (days)	D_f	R_g (Å)	Porosity[b] ϵ (%)	D_{eff} (nm)	E_{act} (H_2) (kJ.mol^{-1})	α H_2/CH_4
$StSiO_2$	0 10 20	1.45 1.65 1.75	20 30 35	35–40	0.5/0.75	5–17[c]	30–50
SiTi10Bu $r_w=1$	4	[d]	[d]	42	0.5/0.75		
SiTi10Bu $r_w=6.4$	4	1.9	51	7	[e]		
SiTi10Pr2	3	1.3	17	27	0.5/0.75	16.3	
SiTi10Bu2	3	1.3	17	28	0.5/0.75	8.4	
SiTi10X	30	2.04	36	2	[e]		200
SiZr10	8	[d]	[d]	16	$\approx$0.6		
SiZr10-2 $r_w=2$	6	1.43	8.4	2	[e]		
SiA110 $r_w=4.6, 70$				1	[e]	9.2	

[a]Prepared from freshly prepared sols.
[b]Porosity ϵ calculated using a skeletal density of 2.2 g.cm^{-3}, 2.36 g.cm^{-3}, 2.40 g.cm^{-3} and 2.31 g.cm^{-3} for amorphous silica, silica/titania, silica/zirconia and silica/alumina, respectively.
[c]Data taken from [34].
[d]No significant scattering.
[e]No PSD defined.

second dipping procedure, this relatively strong decrease in permeation can not be explained by a second comparable thick layer, but it indicates that indeed defects, with very high permeation rates compared to the microporous top-layer, have been eliminated.

The higher separation factor for H_2/CH_4 compared to H_2/CO_2 as found for membrane Al3-Si2-A (Fig. 14) is in agreement with gas separation properties for a series of binary gas mixtures with H_2 as reported elsewhere [32]. Generally it is found that the separation factor increases in the order $H_2/CO_2 < H_2/CH_4 < H_2$/propene $< H_2$/isobutane. Differences in molecular size play a role in the separation mechanism (the kinetic diameter of methane is larger than for carbon dioxide (0.33 nm and 0.38 nm, respectively [51]), but also sorption phenomena are important. The exact mechanism is discussed in an extensive gas transport study [32,33].

From the gas transport data summarized in Table 4 it is clear that microporous membranes have been obtained from both silica and binary sols. As has been shown before [37], microporous non-supported membranes have been obtained from a range of fractal polymeric sols. A comparison of some representative non-supported and supported membrane characteristics is given in Table 5.

For standard silica modified membranes, the corrected activation energies are in the order of 5–17 kJ.mol^{-1} for hydrogen. This activation energy can be regarded as a tool to judge membrane quality, as will be shown elsewhere [32].

Using this criterium, the binary membranes are within the quality range observed for silica modified membranes. Improved transport properties are observed for both membranes corresponding with non-supported membranes with high porosities (''$StSiO_2$'', ''SiTi10Pr2'' and ''SiTi10Bu2'') and non-supported membranes with low porosities (''SiTi10X'' and ''SiA110''). The permeation rates, which are in the order of 15×10^{-7} mol.m^{-2}.s^{-1}.Pa^{-1} for H_2 at 200°C for ''$StSiO_2$'', however, are a factor 3–10 lower for the latter two membranes, as can be seen in Table 4. These low permeation rates are approximately proportional to the difference in porosity found for these non-supported membranes prepared from these sols compared to pure silica.

These very interesting, molecular sieve-like, transport properties, show that the pore size of the supported membranes is very small, and in the order of the pore sizes found for the non-supported membranes. Based on the relatively high permeation rates of these membranes, and on the order of the activation energy, it can be concluded that transport takes place through micropores, and not through a dense layer. In comparison with dense quartz glass (activation energies of 38 kJ.mol^{-1} for hydrogen [52]), the activation energy

for permeation is low. Moreover, the permeation rates found for the sol-gel derived membranes are high. The hydrogen permeation through dense quartz glass at 500°C, with a layer thickness of 0.1 μm, has found to be in the order of 1×10^{-8} mol.m^{-2}.s^{-1}.Pa^{-1} [53]; at 200°C the permeation will be of the order of 2×10^{-10} mol.m^{-2}.s^{-1}.Pa^{-1}., which is more than a factor 1000 lower than for hydrogen permeation for the sol-gel derived membranes described in this work.

The relation between fractal dimension, porosity of the non-supported membranes and supported membrane properties is not straightforward.

Very low porosities for non-supported membranes have been found for both sols with high fractal dimensions (samples "SiTi10Bu, $r_w=6.4$" and "SiTi10X"), moderate fractal dimension ("SiZr10-2") and sols with polymers too small to show significant scattering ("SiAl10"). Relatively high porosities have been found for samples with low fractal dimensions ("SiTi10Bu, $r_w=1$" and "SiZr10") and moderate fractal dimensions ("$StSiO_2$", "SiTi10Bu2" and "SiTi10Pr2").

The sol properties of supported SiO_2/TiO_2 modified membranes using sols "SiTi10Pr2" and "SiTi10Bu2" are comparable with standard silica sols. It looks therefore not surprisingly that membrane properties are comparable as well. However, supported membranes using "SiTi10X" and "SiAl10, $r_w=4.6, 70$" also give rise to comparable gas transport properties. The sol structures, however, are significantly different. "SiTi10X" has a fractal dimension of 2.04, which is relatively high compared to the silica sols. The fractal dimension of the corresponding TiO_2 sol used as one of the components in this mixed sol was 2.2. The SiO_2 sol used for the mixed sol consists of very small oligomers; sols prepared under comparable conditions showed no scattering with SAXS. Although the sol age for the measurement was 30 days, it is not expected to deviate significantly from a freshly prepared sol, since the concentration is very low, which effectively retards further growth [36]. Since scattered intensity of TiO_2 is stronger than for SiO_2, the TiO_2 signal will dominate the spectrum. The formation of microporous materials from sols with such a high fractal dimension is not expected directly from the analysis based on fractal structures using Eqs. (2) and (3). A possible explanation that for this case indeed a microporous consolidated material was obtained is that the sol consists of a distribution of fractal structures. The main phase consists of the very weakly branched silica and a minor phase consists of the branched TiO_2. This also may explain the rather low permeation rate.

The membrane prepared from "SiAl10 $r_w=4.6, 70$" showed a very low permeation rate. The structure of the used sol is probably oligomeric since no scattering was observed. Interpenetration of these oligomers therefore results in a low porosity.

Further, we have observed that increasing the water content in the binary sol synthesis always leads to less porous materials [37], which is very remarkable, since the fractal dimensions increase [36]. Obviously, the addition of more water for the binary sols results in internal condensation of the already formed structures. If no further growth takes place, the final radius of gyration can still be low. In spite of the fact that interpenetration of these denser structures is hindered, denser consolidated structures are formed.

For an explanation of the observation that dense materials are obtained from sols with high fractal dimension, the size of the polymers has to be taken into account as well. As can be seen from Eq. (2), the number of intersections $M_{1,2}$ for sols with $D_f>1.5$, which is the case for this discussion, increases as r is increased. The tendency to interpenetrate is therefore low. The porosity of the individual polymers, however, decreases for higher fractal dimensions. The cumulative effect can be an almost dense system. Obviously the effect of the decreased porosity of the individual structures prevails in the formation mechanism, and the tendency to interpenetrate is less important.

The discussed observations show that a prediction of the porosity of the consolidated material based on fractal dimension and interpenetration alone is difficult. The influence of support constraints may be important, because these will tend to hinder densification as discussed before. When evaporation takes place very fast due to the thin layer, this will result in a reduced time in which further condensation takes place, so promoting the formation of less porous materials with small micropores. So the ratio's of condensation rate, penetration rate and drying rate are important.

5. Conclusions

High quality γ-alumina membranes are used for the modification with microporous top-layers, resulting in enhanced gas transport properties.

Non-supported γ-alumina top-layers have a porosity of 57% after calcination at 600°C, with a pore radius (cylindrical geometry) of around 2.2 nm. Supported membranes showed a slightly higher pore radius of 2.5 nm. This difference is attributed to support constraints which hinder densification.

The top-layer of supported γ-alumina membranes is 7–10 μm after three dipping procedures with boehmite dip solutions. A very fine surface roughness of 40 nm was obtained, and is necessary to obtain high quality microporous top-layers in a subsequent processing step.

Microporous silica top-layers have thicknesses in the order of 60–100 nm. The surface roughness was not further decreased.

Microporous top-layers with interesting, molecular sieve-like gas transport properties have been obtained by modification with a broad range of sol structures; from oligomeric structures which show no scattering with SAXS, to polymeric sols with fractal dimensions to 2.04.

Activation energies for hydrogen permeation are in the order of 5–17 kJ.mol^{-1}. typical permeation rates for hydrogen at 200°C are in the order of 10×10^{-7} mol.m^{-2}.s^{-1}.Pa^{-1}. Gas separation factors for H_2/CH_4 up to 200 have been found.

Repair of defects in microporous membranes was performed successfully by a single extra dipping step.

Acknowledgements

Special thanks to A.A. ten Hoeve and P.J.A.M. Blankenvoorde for their help related with synthesis and characterization of microporous membranes. A.J.H. van den Berg and M.A. Smithers of the Center for Materials Research (CMO) of the University of Twente are thanked for performing respectively the SAM and FE-SEM analysis. G.W. Koebrugge is acknowledged for his help with the AFM experiments.

Appendix: Support correction

Appendix: support correction Corrections for the influence of the support system on the permeation of the microporous top-layer have to be performed to calculate the real pressure drop over the top-layer. In this work, the support system is the γ-alumina membrane, which is a composite membrane consisting of a γ-alumina top-layer on an α-alumina support. We will further refer to the γ-alumina membrane as "support", and to the microporous silica layer as "top-layer". The corrections were performed by the series model [54,55], which requires knowledge of the permeation characteristics of the support. It is assumed that the resistance for permeation for the system is a series process of the support resistance and the top-layer resistance, where the permeation is a reciprocal resistance:

$$\frac{1}{F_{0,\text{membrane}}}=\frac{1}{F_{0,\text{top-layer}}}+\frac{1}{F_{0,\text{support}}} \tag{6}$$

Support characteristics were determined with H_2 permeation at room temperature. The total support permeation can then be expressed as:

$$F_{0,\text{support}}=\alpha_s+\beta_s.P_{av} \tag{7}$$

where α_s expresses the Knudsen component, $\beta_s.P_{av}$ expresses the Poiseuille (laminar) flow component, and P_{av} is the average pressure ($P_{high}-P_{low}$). For the supports used in this work, mean values for α_s and β_s for hydrogen at 25°C are, respectively, 62

Table 6
Example support correction H_2 permeation data for membrane Al3-Si2-A

Input						Results		
Temperature (°C)	P_{high} (bar)	Φ (mol.s^{-1}) $\times10^{-6}$	α_s^a	β_s^b	$F^a_{0,\text{membrane}}$	P_i (bar)	$F^a_{0,\text{support}}$	$F^a_{0,\text{top}}$
50	2.065	7.11	44.0	3.2	1.80	0.0944	44.1	1.88
250	0.71	7.11	35.0	1.4	6.77	0.118	34.6	8.42
250	1.995	27.9	35.0	1.4	7.30	0.429	34.8	9.23

[a] 10^{-7} mol.m^{-2}.s^{-1}.Pa^{-1}.
[a] 10^{-12} mol.m^{-2}.s^{-1}.Pa^{-2}.

$ml.min^{-1}.cm^{-2}.bar^{-1}$ ($\equiv 46.1\times10^{-7}$ $mol.m^{-2}.s^{-1}.Pa^{-1}$) and 5 $ml.min^{-1}.cm^{-2}.bar^{-2}$ ($\equiv 3.7\times10^{-12}$ $mol.m^{-2}.s^{-1}.Pa^{-2}$). The values for α_s and β_s for other gases and/or different temperatures are calculated from the measured hydrogen data from the temperature dependency of the Knudsen diffusion component(α_s) and the laminar flow component(β_s) [54]. From experiments with He and H_2 between 25°C and 200°C it was found that the accuracy in calculating these flow components at different temperatures according to this estimate is around 5–10% [56]. The pressure at the interface (P_i) of the top-layer (microporous silica) and the support (γ-alumina membrane) can than be calculated by [54,55]:

$$P_i = \frac{-\alpha_s + \left[\alpha_s^2 + \beta_s\left(\beta_s.P_l^2 + 2.\alpha_s.P_l + 2.\frac{\Phi}{S}\right)\right]^{1/2}}{\beta_s} \quad (8)$$

where P_l is the pressure at the permeate side of the membrane, S is the permeation area and Φ is the flow rate. The support permeation for the *actual* experiment is then given by:

$$F_{0,support} = \frac{\Phi}{S.(P_i - P_l)} \quad (9)$$

Since now both the total permeation ($F_{0,membrane}$) and the support permeation ($F_{0,support}$) are known, Eq. (6) can be used to calculate the top-layer permeation $F_{0,top\text{-}layer}$.

For example, some support correction data of membrane Al3-Si2-A (Fig. 13) is given in Table 6. The permeation area (S) is 1.911 cm^{-2} and the pressure at the down-stream side (P_l) is 0.01 bar. The values of α_s and β_s at 50°C and 250°C are calculated as described before from the mean values; the viscosity (η) of H_2 at 25, 50 and 250°C is, respectively, 0.889×10^{-5}, 0.944×10^{-5} and 1.305×10^{-5} $N.s.m^{-2}$ [57].

P_i, calculated from Eq. (8) using the corresponding flow rates (Φ), can be substituted in Eq. (9) to obtain the actual support permeation $F_{0,support}$.

From the input data in Table 6 it can be clearly seen that increasing the temperature results in:

(i) Decreased support permeation rates, because both α_s and β_s decrease.

(ii) Increased total permeation rates, due to activated transport.

(iii) Decreased pressure drops over the membranes for the same gas flow. The relative pressure drop over the support (defined as $P_i - P_l)/(P_{high} - P_l$) increases; at 50°C this is only 4%, while this is 15% at 250°C (same gas flow).

Therefore, support correction is larger at higher temperatures.

References

[1] R.R. Bhave, Inorganic Membranes: Synthesis, Characteristics and Applications, Van Nostrand Reinhold, New York, 1991.

[2] K.S.W. Sing, D.H. Everett, R.A.W. Haul, L. Moscou, R.A. Pierotti, J. Rouquérol and T. Siemieniewska, Reporting physisorption data for gas/solid systems with special reference to the determination of surface area and porosity (IUPAC Recommendations 1984), Pure and Appl. Chem., 57 (1985) 603–619.

[3] A.J. Burggraaf, K. Keizer, R.S.A. de Lange, Z.A.E.P. Vroon and V.T. Zaspalis, Ceramic Membranes for Separations and Reactions, in J.B. Higgins, R. von Balmoos and M.M.J. Treacy (Eds.), Proceedings of the 9th International Zeolite Conference, Montreal, Canada, July 5–10, 1992, Butterworth-Heinemann, Stoneham, MA, 1993, pp. 47–71.

[4] R.J.R. Uhlhorn, K. Keizer and A.J. Burggraaf, Gas transport and separation with ceramic membranes. Part II: Synthesis and separation properties of microporous membranes, J. Membrane Sci., 66 (1992) 271–288.

[5] S. Kitao, H. Kameda and M. Asaeda, Gas separation by thin porous silica membrane of ultra fine pores at high temperature, Membrane, 15 (1990) 222–227.

[6] R.S.A. de Lange, J.H.A. Hekkink, K. Keizer and A.J. Burggraaf, Preparation and characterization of microporous sol-gel derived membranes for gas separation applications, in M.J. Hampden-Smith, W.G. Klemperer and C.J. Brinker (Eds.), Better Ceramics through Chemistry V, Mater. Res. Symp. Proc., Vol. 271, Materials Research Society, Pittsburgh, 1992, pp. 505–510.

[7] C.J. Brinker, T.L. Ward, R. Sehgal, N.K. Raman, S.L. Hietala, D.M. Smith, D.-W. Hua and T.J. Headley, Ultramicroporous silica-based supported inorganic membranes, J. Membrane Sci., 77 (1993) 165–179.

[8] A. Julbe, C. Guizard, A. Larbot, L. Cot and A. Giroir-Fendler, The sol-gel approach to prepare candidate microporous inorganic membranes for membrane reactors, J. Membrane Sci., 77 (1993) 137–153.

[9] R.S.A. de Lange, K.-N.P. Kumar, J.H.A. Hekkink, G.M.H. van de Velde, K. Keizer, A.J. Burggraaf, W.H. Dokter, H.F. van Garderen and T.P.M. Beelen, Microporous SiO_2 and SiO_2/MO_x (M = Ti, Zr, Al) for ceramic membrane applications; A microstructural study of the sol-stage and the consolidated state, 2 (1994) 489–495.

[10] R.S.A. de Lange, Microporous Sol-gel Derived Ceramic Membranes for Gas Separation; Synthesis, Gas Transport and Separation Properties, Ph.D. Thesis, University of Twente, Enschede, The Netherlands, 1993.

[11] T. Okubo and H. Inoue, Single Gas permeation through porous glass modified with tetraethoxysilane, AIChE J., 35 (1989) 845–848.

[12] G.R. Gavalas, C.E. Megiris and S.W. Nam, Deposition of H_2-permselective SiO_2 films, Chem. Eng. Sci., 44 (1989) 1829–1835.

[13] M. Tsapatsis, S. Kim, S.W. Nam and G. Gavalas, Synthesis of hydrogen permselective SiO_2, TiO_2, Al_2O_3 and B_2O_3 membranes from the chloride precursors, I EC Res., 30 (1991) 2152–2159.

[14] S. Kitao and M. Asaeda, Gas separation performance of thin porous silica membranes prepared by sol-gel and CVD-methods, Key Eng. Mater., 61/62 (1991) 267–272.

[15] C.E. Megiris and J.H.E. Glezer, Synthesis of H_2-permselective membranes by modified chemical vapor deposition. Microstructure and permselectivity of SiO_2/C/vycor membranes, Ind. Eng. Chem. Res., 31 (1992) 1293–1299.

[16] Y.S. Lin, Chemical and Electrochemical Vapour Deposition of Zirconia-Yttria Solid Solutions in Porous Ceramic Media, Ph.D. Thesis, University of Twente, Enschede, The Netherlands, 1992.

[17] Y.S. Lin and A.J. Burggraaf, CVD of solid oxides in porous substrates for ceramic membrane modification, AIChE J., 38 (1992) 445–454.

[18] Y.S. Lin and A.J. Burggraaf, Experimental studies on pore size changes of porous ceramic membranes after modification, J. Membrane Sci., 79 (1993) 65–82.

[19] G.Z. Cao, J. Meijerink, H.W. Brinkman, K.J. de Vries and A.J. Burggraaf, Growth of thin dense gas-tight (Tb,Y)-ZrO_2 films by electrochemical vapour deposition, J. Mater. Chem., 3 (1993) 773–774.

[20] J. Koresh and A. Soffer, Study of molecular sieve carbons. Part 1. Pore structure, gradual pore opening and mechanism of molecular sieving, J. Chem. Soc. Faraday Trans., 76 (1980) 2457–2471.

[21] M. Bhandarkar, A.B. Shelekhin, A.G. Dixon and Y.H. Ma, Adsorption, permeation and diffusion of gases in microporous membranes. I. Adsorption of gases on microporous glass membranes, J. Membrane Sci., 75 (1992) 221–231.

[22] A.B. Shelekhin, A.G. Dixon and Y.H. Ma, Adsorption, permeation, and diffusion of gases in microporous membranes. II. Permeation of gases in microporous glass membranes, J. Membrane Sci., 75 (1992) 232–244.

[23] E.R. Geus, M.J. den Exter and H. van Bekkum, Synthesis and characterization of zeolite (MFI) membranes on porous ceramic supports, J. Chem. Soc. Faraday Trans. 1, 88 (1992) 3102–3109.

[24] W.J.W. Bakker, G. Zheng, F. Kapteijn, M. Makkee, J.A. Moulijn, E.R. Geus and H. van Bekkum, Single and Multi-component Transport through Metal-Supported MFI Zeolite Membranes, in M.P.C. Weynen and A.A.H. Drinkenburg (Eds.), Precision Process Technology; Perspectives for Pollution Prevention, Kluwer Academic Publishers, Dordrecht, The Netherlands, 1993, pp. 425–436.

[25] E.R. Geus, Preparation and Characterization of Composite Inorganic Zeolite Membranes with Molecular Sieve Properties, Ph.D. Thesis, Technical University of Delft, Delft, The Netherlands, 1993.

[26] M.D. Jia, K.V. Peinemann and R.D. Behling, Ceramic zeolite composite membranes. Preparation, characterization and gas permeation, J. Membrane Sci., 82 (1993) 15–26.

[27] A.F.M. Leenaars, K. Keizer and A.J. Burggraaf, The preparation and characterization of alumina membranes with ultra-fine pores. Part I Microstructural investigations on non-supported membranes, J. Mater. Sci., 19 (1984) 1077–1088.

[28] A.F.M. Leenaars and A.J. Burggraaf, The preparation and characterization of alumina membranes with ultrafine pores. 2. The formation of supported membranes, J. Colloid Interface Sci., 105 (1985) 27–40.

[29] R.J.R. Uhlhorn, M.H.B.J. Huis in 't Veld, K. Keizer and A.J. Burggraaf, Synthesis of ceramic membranes. Part I. Synthesis of non-supported and supported γ-alumina membranes without defects, J. Mater. Sci., 27 (1992) 527–537.

[30] J. Kärger and D.M. Ruthven, Diffusion in Zeolites and other Microporous Materials, Wiley, New York, 1992.

[31] M.F.M. Post, Diffusion in Molecular Sieves, in H. van Bekkum, E.M. Flanigen and J.C. Jansen (Eds.), Introduction to Zeolite Science and Practice, Elsevier, Amsterdam, 1991, pp. 391–443.

[32] R.S.A. de Lange, J.H.A. Hekkink, K. Keizer and A.J. Burggraaf, Permeation and separation studies on microporous sol-gel modified ceramic membranes, Microporous Solids, (1994) submitted.

[33] R.S.A. de Lange, K. Keizer and A.J. Burggraaf, Analysis and the theory of the gas transport mechanisms in microporous sol-gel derived membranes, J. Membrane Sci., (1995) accepted.

[34] C.J. Brinker, G.C. Frye, A.J. Hurd and C.S. Ashley, Review of sol-gel thin film formation, J. Non-Cryst. Solids, 147/148 (1992) 424–436.

[35] B.B. Mandelbrot, The Fractal Geometry of Nature, Freeman, San Francisco, CA, 1983.

[36] R.S.A. de Lange, J.H.A. Hekkink, K. Keizer and A.J. Burggraaf, Polymeric silica based sols for membrane modification applications; Sol-gel synthesis and characterization with SAXS, J. Non-Cryst. Solids, (1994) submitted.

[37] R.S.A. de Lange, J.H.A. Hekkink, K. Keizer and A.J. Burggraaf, Microstructural characterization of non-supported microporous ceramic membrane toplayers obtained by the sol-gel process, J. Non-Cryst. Solids, (1994) submitted.

[38] G.C. Frye, A.J. Ricco, S.J. Martin and C.J. Brinker, Characterization of the surface area and porosity of sol-gel films using SAW devices, in C.J. Brinker, D.E. Clark and D.R. Ulrich (Eds.), Better Ceramics Through Chemistry III, Mater. Res. Soc. Symp. Proc., Vol. 121, Materials Research Society, Pittsburgh, PA, 1988, pp. 349–354.

[39] E.P. Barrett, L.G. Joyner and P.P. Halenda, The determination of pore volume and area distributions in porous substances. I. Computations from nitrogen isotherms, J. Am. Chem. Soc., 73 (1951) 373–380.

[40] S.J. Gregg and K.S.W. Sing, Adsorption, Surface Area and Porosity, Academic Press, London, 1982, Chapter 4.
[41] G.Z. Cao, J. Meijerink, H.W. Brinkman and A.J. Burggraaf, Permporometry study on the size distribution of active pores in porous ceramic membranes, J. Membrane Sci., 83 (1993) 221–235.
[42] L.E. Davis, N.C. McDonald, P.W. Palmberg, G.E. Riach and R.E. Weber, Handbook of Auger Spectroscopy, 2nd edition, Physical Electronics, Edina M.N., 1987.
[43] D. Briggs and M.P. Seah, Practical Surface Analysis by Auger and X-ray Spectroscopy, Wiley, Chichester, 1983.
[44] F.P. Cuperus, D. Bargeman and C.A. Smolders, Permporometry. The determination of the size distribution of active pores in UF membranes, J. Membrane Sci., 71 (1992) 57–67.
[45] V.T. Zaspalis, Catalytically Active Ceramic Membranes: Synthesis, Properties and Reactor Applications, Ph.D. Thesis, University of Twente, Enschede, The Netherlands, 1990.
[46] University of Twente, The Netherlands, unpublished results.
[47] K.-N.P. Kumar, K. Keizer, A.J. Burggraaf, T. Okubo and H. Nagamoto, Synthesis and textural properties of unsupported rutile (TiO_2) membranes, J. Mater. Chem., 3 (1993) 923–929.
[48] V.T. Zaspalis, On the Influence of Surface Roughness on Membrane Formation, Internal Report CT92/041/128, University of Twente, Enschede, The Netherlands, 1992.
[49] K.-N.P. Kumar, Nanostructured Ceramic Membranes. Layer and texture formation, Ph.D. Thesis, University of Twente, Enschede, The Netherlands, 1993, Chapter 2.
[50] P.C. Zalm, Quantitative sputtering, Surface Interface Anal., 11 (1988) 1–24.
[51] D.W. Breck, Zeolite Molecular Sieves: Structure, Chemistry and Use, Wiley, New York, 1973, p. 636.
[52] R.W. Lee, Diffusion of hydrogen in natural and synthetic fused quartz, J. Chem. Phys., 38 (1963) 448–455.
[53] T. Ioannides and G.R. Gavalas, Catalytic isobutane dehydrogenation in a dense silica membrane reactor, J. Membrane Sci., 77 (1993) 207–220.
[54] R.J.R. Uhlhorn, Ceramic Membranes for Gas Separation: Synthesis and Transport Properties, Ph.D. Thesis, University of Twente, Enschede, The Netherlands, 1990.
[55] Y.S. Lin and A.J. Burggraaf, Preparation and characterization of high-temperature thermally stable alumina composite membrane, J. Am. Ceram. Soc., 74 (1991) 219–224.
[56] R.S.A. de Lange, unpublished results.
[57] C.F. Beaton and G.F. Hewitt, Physical Property Data for the Design Engineer, Hemisphere, New York, 1989.